Acta Materialia 292 (2025) 121031

Contents lists available at ScienceDirect

Acta Materialia

journal homepage: www.elsevier.com/locate/actamat

Full length article

Machine learning guided design of RE-Fe-B(RE=PrNd,La,Ce) with comprehensive high performance

Zheng Wang [a,b], Shiyi Zhang [a,d], Jing Wang [a,b,*], Ming Zhang [c], Yunzhong Chen [a,b], Baohe Li [d], Tongyun Zhao [a,e], Minggang Zhu [f,*], Fengxia Hu [a,b,g,*], Baogen Shen [a,b,e,h,*], Wei Li [f]

[a] *Beijing National Laboratory for Condensed Matter Physics, Institute of Physics, Chinese Academy of Sciences, Beijing, 100190, PR China*
[b] *School of Physical Sciences, University of Chinese Academy of Sciences, Beijing, 101408, PR China*
[c] *School of Science, Inner Mongolia University of Science and Technology, Baotou, Inner Mongolia 014010, PR China*
[d] *School of Physics, Beijing Technology and Business University, Beijing 100048, PR China*
[e] *Ganjiang Innovation Academy, Chinese Academy of Sciences, Ganzhou, Jiangxi, 341000, PR China*
[f] *Division of Function Materials, Central Iron and Steel Research Institute, Beijing 100081, PR China*
[g] *Songshan Lake Materials Laboratory, Dongguan, Guangdong, 523808, PR China*
[h] *Ningbo Institute of Materials Technology & Engineering, Chinese Academy of Sciences, Ningbo, Zhejiang, 315201, PR China*

ARTICLE INFO

Keywords:
Machine learning
REFeB
High-abundance rare earth elements
Electronegativity

ABSTRACT

The optimization of high-abundance REFeB (RE=PrNd,La,Ce) permanent magnets has been a significant research focus, but traditional trial-and-error methods are challenging due to high costs and time consumption. Here, we propose a machine-learning approach to accelerate the design of melt-spun high-abundance (PrNd,La,Ce)-Fe-B ribbons based on the database incorporating elemental electronegativity with the composition and magnetic performance collected from literature. By combining heuristic optimization algorithms and ensemble strategies, we developed accurate and robust machine learning models, allowing for rapid evaluation of comprehensive magnetic performance across different compositions in high-dimensional data spaces and discovering high-performance REFeB permanent magnets with high-abundance rare earth elements. Utilizing the established models, by balancing three magnetic properties of coercivity, remanence and maximum magnetic energy product, we discovered a compositional range with optimal overall magnetic performance and high proportions of high-abundance rare earth elements (up to 40 % La and 20 % Ce of the total rare earth content) for the magnets of $(PrNd_xLa_yCe_{1-x-y})_{12}Fe_{82}B_6$, which were verified by experiments with accuracies exceeding 90 %. Within this range, four cost-effective compositions were identified, among which the best composition, $(Pr,Nd)_{8.1}La_{3.6}Ce_{0.3}Fe_{82}B_6$, achieved a 31.3 % cost reduction while retaining 86.4 % of the magnetic performance. This study advances the optimization of REFeB compositions with high-abundance rare earth elements, demonstrating the enormous potential of machine-learning approach in the design and development of high-performance and cost-effective REFeB permanent magnets.

1. Introduction

Since first discovered in 1984, Sagawa et al. [1] NdFeB magnets have rapidly become one of the most widely utilized rare-earth permanent magnets, renowned for their exceptional comprehensive magnetic performance. They have emerged as a cornerstone in the industrial sector, finding extensive applications in various fields such as the automotive industry, wind power generation, and clean energy, constituting over half of the market value in the magnet industry [2,3] Building on the success of NdFeB magnets, the development of other REFeB permanent magnets gained increasing attention, particularly as part of efforts to reduce reliance on critical rare earth elements, considerable endeavors have been devoted to developing high-performance REFeB magnets [4–6] The common magnetic properties used to evaluate the magnetic performance of REFeB include remanence B_r, intrinsic coercivity H_{cj} and maximum magnetic energy product $(BH)_{max}$. The factors influencing on

* Corresponding authors at: Beijing National Laboratory for Condensed Matter Physics, Institute of Physics, Chinese Academy of Sciences, Beijing 100190, PR China; Division of Function Materials, Central Iron and Steel Research Institute, Beijing 100081, PR China.

E-mail addresses: wangjing@iphy.ac.cn (J. Wang), mgzhu@126.com (M. Zhu), fxhu@iphy.ac.cn (F. Hu), shenbg@iphy.ac.cn (B. Shen).

https://doi.org/10.1016/j.actamat.2025.121031
Received 9 September 2024; Received in revised form 7 April 2025; Accepted 9 April 2025
Available online 10 April 2025

the magnetic performance of REFeB permanent magnets are diverse and complex [7]. Variations in the magnet's elemental substitutions and atomic percentages, as well as its microstructures and manufacturing processes, can all induce changes in magnetic performance. Moreover, in pursuit of cost reduction and balancing rare earth resources, researchers are dedicated to substituting Pr and Nd with high-abundance rare earth elements, particularly La and Ce, [8–11] which brought the problem of the decline in magnetic performance. Hence, the design of high abundant REFeB permanent magnets that maintain both high levels of high-abundance rare earth element substitution and relatively optimal magnetic properties continues to be a pivotal area of study. Almost all rare earth elements can form the $RE_2Fe_{14}B$ phase, presenting numerous opportunities for compositional design in high abundant REFeB magnets, but also introducing issues related to high experimental costs and time consumption. The traditional trial-and-error approach encounters challenges in navigating such an expansive search space (Supplementary materials, Note1). As a result, there exists a pressing requirement for an innovative, efficient, and economical approach to investigate the magnetic performance of high abundant REFeB permanent magnets.

As an emerging and innovative methodology, machine learning has gradually integrated into academic research, marking a new paradigm in scientific research within materials science. Grounded in statistical theory, machine learning employs statistical models to identify patterns and relationships within data, enabling subsequent inferences and predictions derived from these recognized patterns. Recently, machine learning has found extensive application in various material science fields including superconductors, [12–16] high-entropy alloys [17–21]. Its rationality and effectiveness have garnered recognition from researchers. In the field of magnetic materials, machine learning has demonstrated success in areas such as two-dimensional magnetic materials [22,23], soft magnetic materials [24,25]. However, its application in permanent magnets remains in the early stages of development. Recently, Xu et al. [26] employed the machine learning methods to develop a physical-based machine-learning model for Sm-Co-based alloys, identifying key physical descriptors that influence the Curie temperature. Choudhary et al. [27] used the machine learning models to predict the grain orientation in sintered FeNdB-type permanent magnets. Despite these advancements, the application of machine learning for compositional optimization of RE-Fe-B permanent magnets, particularly with a focus on substituting high-abundance rare-earth elements such as La and Ce, still remains limited.

In this study, we introduce a novel machine-learning framework that combines heuristic optimization algorithms with ensemble strategies. we applied machine learning methods to melt-spun REFeB (RE=PrNd, La,Ce) ribbons by comprehensively evaluating three magnetic properties of high abundant REFeB magnets: coercivity(H_{cj}), remanence(B_r), and maximum energy product($(BH)_{\max}$). To effectively enhance the model accuracy, we combined heuristic optimization algorithms with traditional machine learning regression models, facilitating rapid and efficient optimization for the regression models. Given the characteristics of small datasets in materials science, ensemble strategies were employed to overcome the limitations of individual models and thus improve the model's generalization ability. Utilizing the established high accuracy and robust models, we predicted and analyzed the relationship between the rare earth content and electronegativity parameters of REFeB magnets and their magnetic performance. Based on the predictive results from the machine learning models, we identified a compositional range with a relatively high La/Ce proportion (25 % to 40 % La, up to 20 % Ce) that exhibits optimal overall magnetic performance for $(PrNd_xLa_yCe_{1-x-y})_{12}Fe_{82}B_6$. The magnetic performance of this region has been experimentally verified with an accuracy (defined as $1 - |M_{exp} - M_{pred}|/M_{exp}$, where M_{exp} represents the experimental value, M_{pred} the predicted one)) of over 90 %. Furthermore, within this region, we identified a composition, $(Pr,Nd)_{8.1}La_{3.6}Ce_{0.3}Fe_{82}B_6$, which retains 86.4 % of overall magnetic performance while reducing material costs by 31.3 % compared to composition without La and Ce. In addition, three other compositions of $(Pr,Nd)_{8.1}La_{3.9}Fe_{82}B_6$, $(Pr,Nd)_{8.4}La_{3.6}Fe_{82}B_6$ and $(Pr,Nd)_{8.1}La_{3.3}Ce_{0.6}Fe_{82}B_6$ were also discovered, which achieve cost reductions of 31.4 %, 28.9 %, and 31.3 % while retaining 80.8 %, 80.7 % and 81.7 % of overall magnetic performance, respectively. These findings provide insights for the optimization of REFeB magnetic materials, presenting a novel approach to the design and development of high-performance and cost-effective REFeB magnets.

2. Methodology

Fig. 1 illustrates the schematic flowchart of the machine learning method used in this work. Our study focuses on high-abundance melt-spun REFeB (RE=PrNd, La, Ce) permanent magnet ribbons. From the published literature (Supplementary Note 2), approximately 400 data entries for (PrNd, La, Ce)-Fe-B were manually collected. The machine learning regression models were evaluated using 16 mainstream algorithms and trained on the constructed database, with the most effective models selected based on their predictive performance. These models were further optimized using three heuristic optimization algorithms, followed by an ensemble strategy to enhance model generalization. The final predictions and analysis were conducted based on the established models. Experimental verification was performed to ensure the accuracy of the model prediction results. The predicted results were further analyzed, leading to the identification of cost-effective compositions with favorable overall magnetic performance.

2.1. Database construction and model evaluation method

We designated the three key magnetic properties—remanence, intrinsic coercivity, and maximum magnetic energy product—as the target variables for our database to comprehensively evaluate the balanced performance of REFeB permanent magnets. To ensure that the selected features encapsulate the intricate relationships between inputs and outputs and enhance model interpretability, we included both the essential compositional content (at %) of REFeB (La, Ce, PrNd, Fe, B, Zr, Nb, Ga, Ti, Co) and electronegativity-related features. This comprehensive feature set aims to provide a deeper understanding of the factors and underlying mechanisms that influence the magnetic properties of REFeB magnets. Previous studies have suggested a potential correlation between electronegativity and the magnetic properties of rare-earth permanent magnets [28]. To explore this, we summarized statistical information related to electronegativity as model features, including the weighted difference [28], the weighted mean and the variance of electronegativity. The detailed calculation methods for electronegativity features, along with the complete set of features used in this work are listed in supplementary materials Table S1.

To better evaluate the machine learning models' predictive performance, we partitioned the data into an 8:2 ratio for training and testing, where the training set was used for model training, and the testing set was used to assess predictive accuracy. To enhance the reliability of the evaluation results, the k-fold cross-validation method ($k = 6$ in this work) was used, which scores k partitions of the dataset, averages their predictive accuracy as the final cross-validation score. We adopted the coefficient of determination (R^2) as the assessment metric for machine-learning regression models, R^2 is computed as:

$$R^2 = 1 - \frac{\sum_{i=0}^{N}(y_i - \hat{y}_i)^2}{\sum_{i=0}^{N}(y_i - \overline{y})^2} \tag{1}$$

where y_i represents the actual value, $\hat{y}_i$ represents the predicted value, $\overline{y}$ represents the mean value, and N represents the number of data samples. R^2 reflects the degree of fit and explanatory power of the regression models with values ranging between 0 and 1, higher R^2 values closer to 1 denote a better model fit to the data.

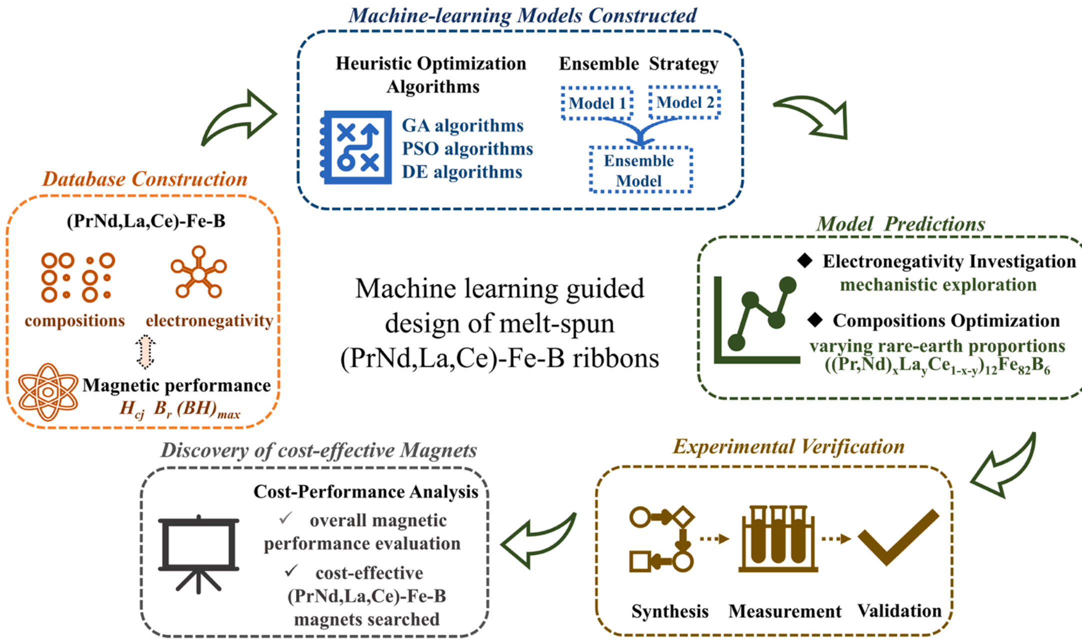

Fig. 1. The design flow f this work.

2.2. Model constructed strategy

2.2.1. Heuristic optimization algorithms

Three heuristic optimization algorithms are employed in this study. Heuristic optimization algorithms are typically designed to efficiently find near-optimal solutions within a search space, making them particularly suitable for complex, non-convex optimization problems with expansive search spaces and intricate nonlinear relationships [29]. These algorithms usually simulate biological phenomena, learning from real-world processes to develop efficient search strategies. This enables the effective identification of near-optimal solutions within acceptable time limits, offering a more effective approach for optimizing machine learning models.

Each machine learning regression model has intrinsic parameters known as hyperparameters, which are not directly learned from the data but are adjusted according to the dataset's characteristics. The optimization process varies across different models (Table S3 in Supplementary Materials), and each model involves multiple hyperparameters that require simultaneous tuning, making the process both complex and computationally demanding. To address this challenge, we employed three heuristic optimization algorithms (Fig. 2) to accelerate model optimization, namely genetic algorithms (GA) [30], differential

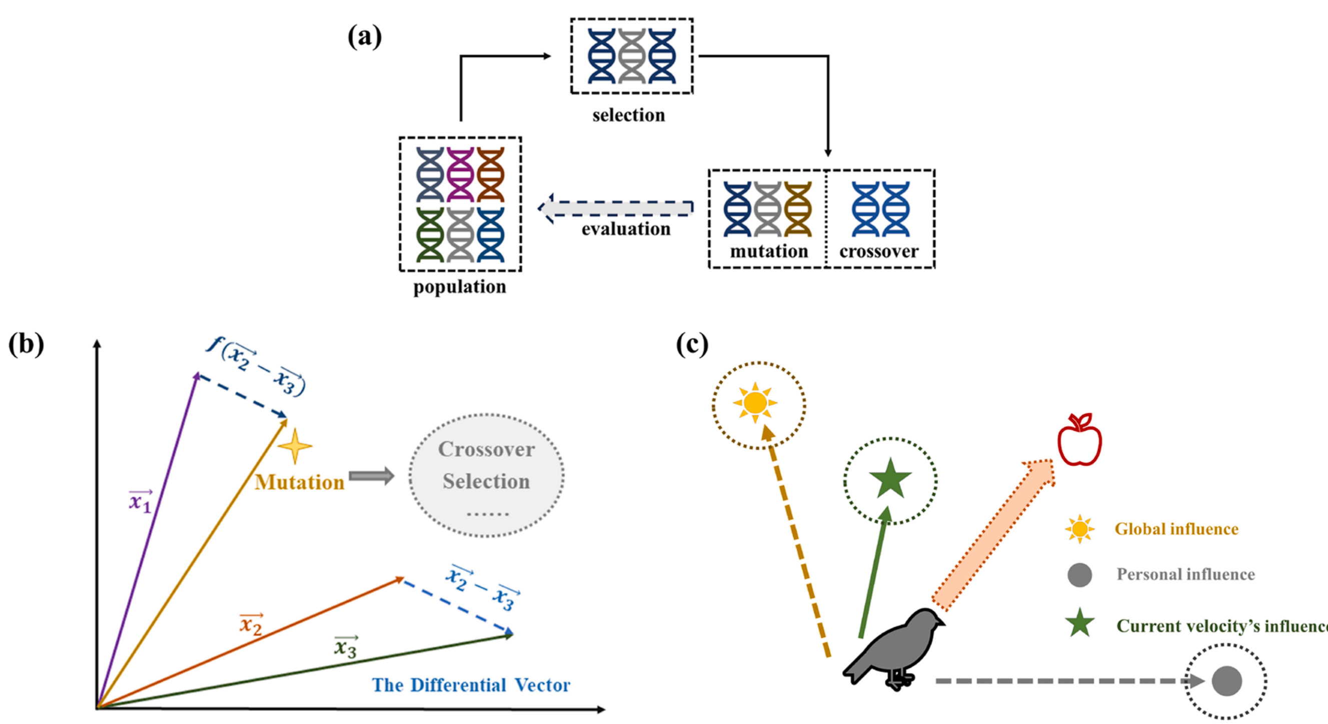

Fig. 2. Optimization process of (a)GA algorithm (b) DE algorithm (c)PSO algorithm.

evolution algorithm (DE) [31], and particle swarm optimization algorithm (PSO) [32], with their biological search strategies detailed in Supplementary Note 3.

2.2.2. Model ensemble strategy

Ensemble methods are also employed to enhance model generalization in this work. The ensemble strategy integrates multiple base models to produce final outputs through techniques such as averaging, bagging, boosting, and stacking. The base models used to build the ensemble model can be homogeneous or heterogeneous. By combining multiple machine learning algorithms, the ensemble method mitigates the weaknesses of individual models, thereby improving generalization [33]. Data acquisition for high-abundance REFeB magnets is challenging due to the high cost and time-consuming nature of experiments, leading to limited datasets and reduced model generalization. To mitigate this, we introduced the ensemble strategy in our machine learning framework, combining predictions from two heterogeneous models to enhance model robustness and reliability.

For each magnetic property, two distinct regression models were selected and optimized. The predictive performance of all six optimized models was evaluated using the coefficient of determination (R^2), confirming their predictive accuracy and consistency. We further compared the R^2 values of the two optimized models for each property, ensuring no significant differences in their predictive performance. This validation step confirmed the ensemble strategy would not compromise the accuracy of the final model. The final ensemble prediction was obtained by averaging the outputs of the two models, which reduced the likelihood of overfitting and consequently improved model robustness and generalization. The ensemble method was implemented for all three magnetic properties, resulting in ensemble models for intrinsic coercivity, remanence, and maximum magnetic energy product. The predictive performance of the ensemble models is analyzed in the following sections.

The machine learning model training, model optimization and predictive analysis were coded in *Python 3.9* with the *scikit-learn* open-source package [34], The heuristic optimization algorithms were implemented with the Python package *pymoo* [35].

2.3. Experimental details

Several experiments were conducted to verify the accuracy of the models. The alloy ingots were produced from the constituent elements using an arc melting technique under a high-purity argon atmosphere. Each ingot weighed 12 g, and all ingots were re-melted at least five times to ensure homogeneity. Ribbons were obtained by induction melting the ingot pieces and then ejecting the melt through an orifice onto the surface of a rotating copper wheel. The surface velocity of the copper wheel was varied in the range of 15–25 m/s to optimize the magnetic properties. Magnetic properties at room temperature were measured using vibrating sample magnetometer (VSM) with a maximum magnetic field of 2 T. The applied field is parallel to the plane of ribbons in order to minimize the demagnetization effect. The measured magnetic properties (H_{cj}, B_r and $(BH)_{\max}$) are obtained by repeating measurements on five different samples under the same experimental conditions.

3. Results and discussion

3.1. Model construction

The model construction process of this work is illustrated in Fig. S3 (see Supplementary materials). To determine the optimal regression models, we trained 16 mainstream machine learning regression algorithms, encompassing a variety of types such as linear regression and support vector machines (Supplementary materials Note 3). Each algorithm was trained to predict intrinsic coercivity, remanence, and maximum energy product of high-abundance REFeB magnets, resulting in a total of 48 model training. The models were preliminarily screened using the cross-validated R^2 score as the evaluation metric. Fig. 3 depicts the varied predictive performance among different regression models. The coefficient of determination (R^2) values closer to 1 indicates a better fit of the model's predictions with the true values, signifying stronger predictive capabilities. The error bars in the graph represent the standard deviation of the 6-fold cross-validation results. We prioritize models with higher R^2 scores and smaller standard deviations, the results show that for coercivity, the models LightGBM (LGBM) and Gradient Boosting (GB) exhibit the highest R^2 values and relatively small standard deviations, identifying them as the top-performing models among the 16 evaluated. Similarly, for remanence, the best-performing models are Gradient Boosting (GB) and XGBoost (XGB), while for maximum magnetic energy product, the models LightGBM (LGBM) and Gradient Boosting (GB) achieve superior predictive accuracy with smaller errors.

Three heuristic optimization algorithms, namely Genetic Algorithm (GA), Particle Swarm Optimization (PSO), and Differential Evolution (DE), were then employed to optimize the six best-performing models selected for each magnetic property. Compared to traditional optimization methods, heuristic algorithms offer a faster and more efficient model optimization approach, achieving significant improvements in both efficiency and accuracy. As demonstrated in our tests, heuristic optimization (GA) reduced optimization time nearly tenfold compared to the traditional Grid Search method (Supplementary Information, Table S6), greatly enhancing computational efficiency. The accuracy of the models also improved through the application of heuristic optimization algorithms, after 18 optimizations, the coefficient of determination (R^2) for all six models was significantly increased, as shown in Table 1.

To evaluate the model's predictive performance, Figs. 4 and 5 compare the predicted values of the models with the actual data. Fig. 4 compares the two optimized models for each magnetic property of REFeB against approximately 80 actual data points from the test dataset. While minor differences exist, the curves exhibit notable consistency between predicted and actual data, which further demonstrates that the six regression models possess high precision and strong predictive capabilities. It is also important to note that the results in Fig. 4 demonstrate the similar predictive performance of both optimized models for each magnetic parameter, indicating comparable predictive abilities without significant differences, which opens up the possibility of the next ensemble step. Besides, we compared the prediction performance of the ensemble models and the optimized models using parity plots (Fig. 5), in which the proximity of data points to the diagonal line indicates how closely the model predictions match the actual results. Before introducing the ensemble strategy, the six optimized regression models clustered closely near the diagonal line. Among them, the best results were observed for B_r, achieving an R^2 of approximately 0.930, with data points distributed closest to the diagonal, demonstrating a strong alignment between predicted and actual values. The results for H_{cj} and $(BH)_{\max}$ were slightly lower but still maintained R^2 values around 0.90, with data points closely distributed around the diagonal as well. For the ensemble models, Table 1 showed the ensemble models had higher R^2 values compared to the individual optimized models, with final R^2 values of 0.927, 0.932, and 0.907 for H_{cj}, B_r, and $(BH)_{\max}$, respectively. As previously discussed, the ensemble strategy can mitigate the limitations of single models, enhancing model generalization and increasing prediction reliability. As shown in Table 1, the R^2 values of the models improved after applying the ensemble strategy, demonstrating the feasibility of our ensemble strategy. We also observed that in Fig. 5, data points in the ensemble models were more concentrated along the diagonal compared to the optimized models before the ensemble, which corresponds to higher R^2 values for the ensemble models, highlighting the advantages of our ensemble strategy in its application of RE-Fe-B permanent magnets.

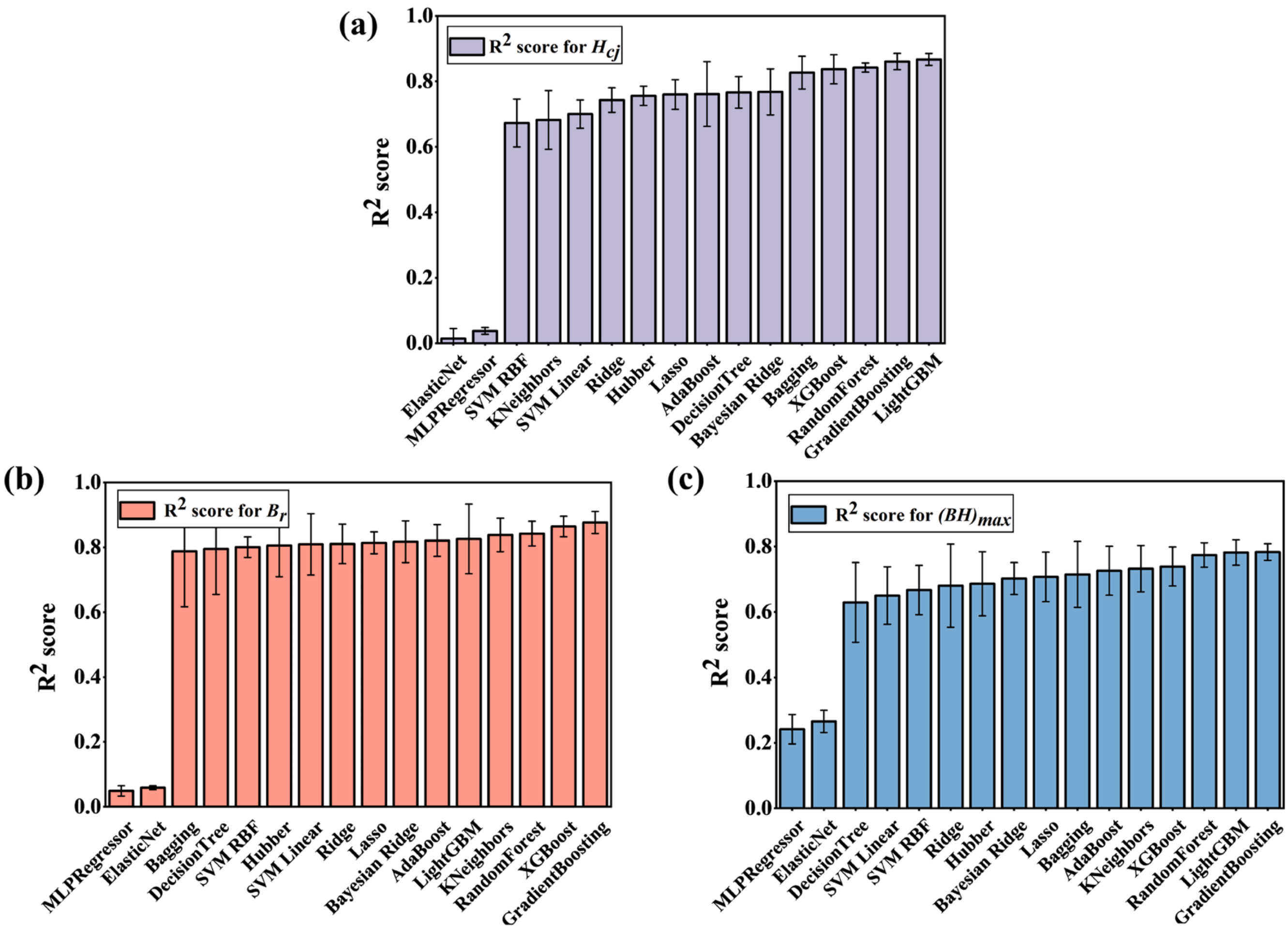

Fig. 3. Performance comparison of various machine learning models for (a) H_{cj} (b) B_r (c) $(BH)_{\max}$ models, assessed using R^2 scores.

Table 1
R^2 scores of different models.

Models		H_{cj}		B_r		$(BH)_{\max}$	
		GB Model	LGBM Model	GB Model	XGB Model	LGBM Model	GB Model
Individual Models	Initial R^2	0.861	0.867	0.877	0.864	0.782	0.783
	GA optimized R^2	0.916	0.919	0.930	0.927	0.893	0.901
	PSO optimized R^2	0.912	0.907	0.909	0.921	0.890	0.888
	DE optimized R^2	0.920	0.906	0.923	0.924	0.884	0.888
	Best optimized Model	DE-GB	GA-LGBM	GA-GB	GA-XGB	GA-LGBM	GA-GB
Ensemble Models	Ensembled R^2	0.927		0.932		0.907	

3.2. Model predictions and analysis

Using the optimized ensemble machine learning models, we predicted and analyzed the performance of high-abundance REFeB magnets based on database variables, including electronegativity parameters and chemical composition. We investigated the relationship between electronegativity parameters and magnetic performance, and predicted the magnetic properties across varying rare earth element contents to identify high-abundance rare earth permanent magnets with optimal overall magnetic performance.

3.2.1. Electronegativity analysis

The feature importance ranking provided by the model (supplementary material, Fig. S2) shows that more than half of the top 10 most important features are related to electronegativity, highlighting the necessity to explore the relationship between electronegativity and magnetic properties. Based on the original composition distribution within the dataset, we generated a virtual dataset encompassing a broad span of chemical compositions for RE-Fe-B magnets. We then calculated the statistical information of electronegativity and compared it with the predicted magnetic properties, the result was presented in the parallel coordinate plot (Fig. 6).

A discernible correlation exists between the electronegativity features of (PrNd,La,Ce)-Fe-B magnets and their magnetic properties. Our models utilized four features derived from electronegativity: the weighted sum of electronegativity (EN_{Wsum}) and the weighted difference of electronegativity (EN_{Wdif}), along with the corresponding variances of these features, denoted as EN_{WSvar} and EN_{WDvar}, respectively. The weighted sum of electronegativity reflects the average level of electronegativity among different elements, while the weighted difference

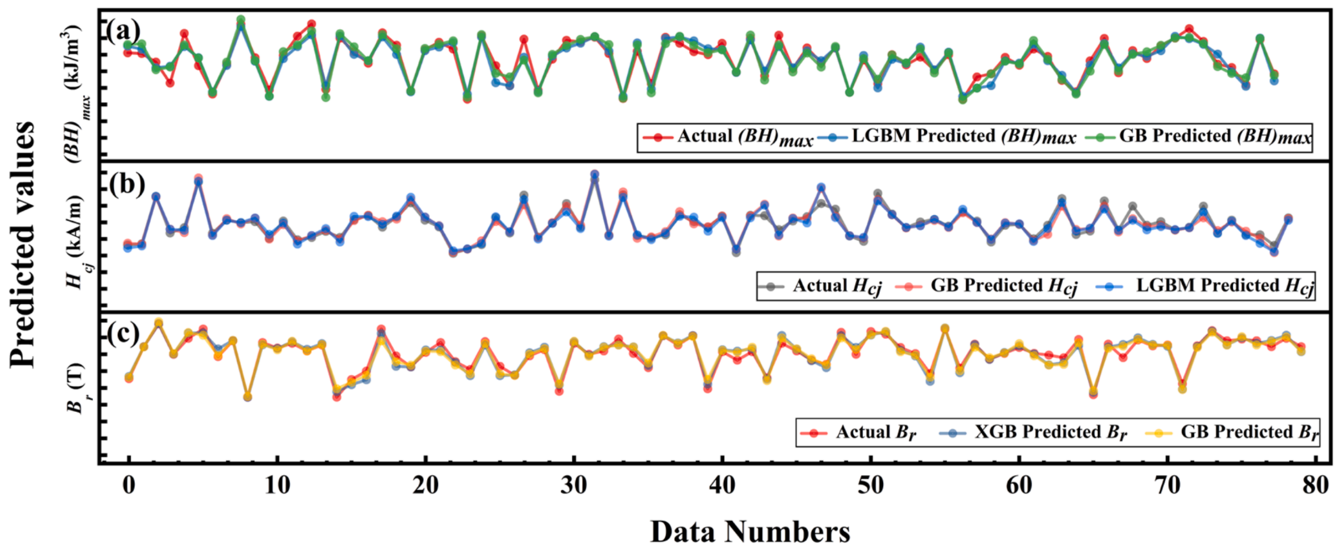

Fig. 4. Comparison of actual and predicted values of the test set data for different magnetic properties using the optimized models: (a) predicted $(BH)_{\max}$ values using LGBM, GB, and actual values (b) predicted H_{cj} values using LGBM, GB, and actual values (c) predicted B_r values using XGB, GB, and actual values.

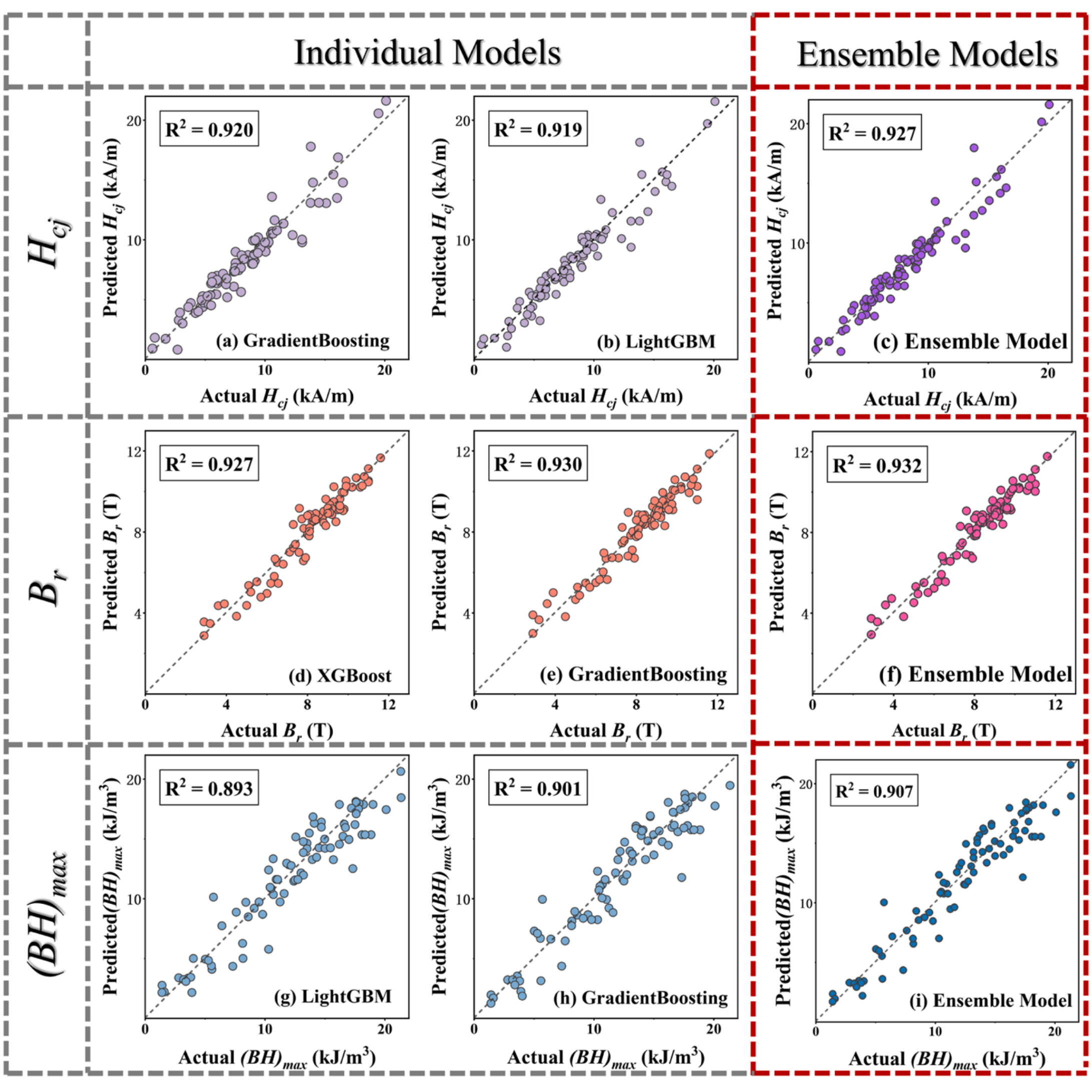

Fig. 5. The parity plots of test set data for H_{cj}, B_r, $(BH)_{\max}$ using different models. (a) LightGBM for H_{cj} (b) GradientBoosting for H_{cj} (c) Ensemble model for H_{cj} (d) XGBoost for B_r (e) GradientBoosting for B_r (f) Ensemble model for B_r (g) LightGBM for $(BH)_{\max}$ (h) GradientBoosting for $(BH)_{\max}$ (i) Ensemble model for $(BH)_{\max}$.

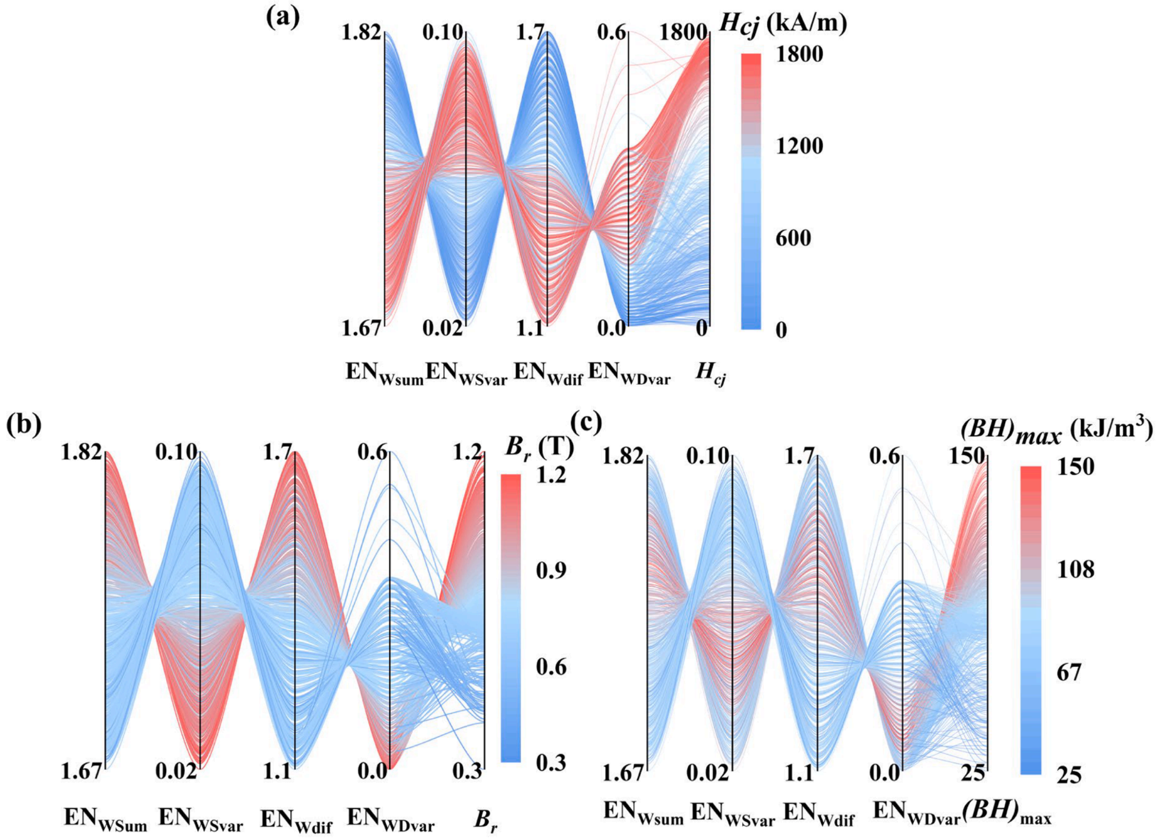

Fig. 6. Parallel coordinate plot demonstrating the relationship between (a) H_{cj} (b) B_r (c) $(BH)_{\max}$ and electronegativity features. Each curve represents an individual data sample, with its intersections on the vertical axes indicating the corresponding values of each variable. The color distribution of the curves reflects the magnitude of the associated magnetic property, allowing the correlation between magnetic properties and electronegativity features to be visually interpreted.

highlights the electronegativity disparity between rare-earth elements and non-rare-earth elements. Variance reflects the degree of variation in electronegativity among different elements in the magnet. The color of the lines in the parallel coordinate plot visually demonstrates the relationship between different factors and the target variables. It is evident that for coercivity and remanence, the color distributions of the four electronegativity features are clearly positively or negatively correlated with the corresponding magnetic performance color distributions, respectively. For remanence, the color distributions of the weighted means of electronegativity (EN_{Wsum} and EN_{Wdif}) align with the remanence color distribution, meaning that high EN_{Wsum} and high EN_{Wdif} correspond to high remanence values, while low EN_{Wsum} and low EN_{Wdif} correspond to lower remanence values. The variance shows an opposite trend, the greater the fluctuation in electronegativity, the lower the remanence value, indicating a significant negative correlation. The trends for coercivity are entirely opposite to those for remanence. High electronegativity variance corresponds to high coercivity values, while the weighted sum and weighted difference of electronegativity show a negative correlation with coercivity. As for the maximum energy product, while a clear positive or negative correlation is not distinctly observed, it is noticeable that there are clear predominant regions within the maximum magnetic energy product area. Specifically, high values of maximum magnetic energy product are observed when EN_{Wsum} lies within the range of approximately 1.75 to 1.79, and EN_{Wdif} is within the range of 1.4 to 1.6. Similarly, prominent intervals are found within the variances; when EN_{WSvar} is within the range of 0.04 to 0.06, and EN_{WDvar} is within the range of 0.06 to 0.14, the maximum magnetic energy product demonstrates high values.

These results show a distinct correlation between the electronegativity of REFeB magnets and their magnetic performance. For different magnetic properties, the electronegativity parameters of REFeB magnets exhibit different patterns. As the essence of machine learning is to extract patterns and relationships from data, direct interpretations cannot be directly obtained from the machine learning model. However, the virtual datasets derived from the predictive results clearly reveal the underlying correlation between the electronegativity parameters and the magnetic properties of REFeB. The electronegativity parameters we designed are based on the chemical composition of the compounds. To some extent, these electronegativity parameters can serve as proxies for the electronic environment of atoms within the compound, as well as the magnetic interactions between them, all of which ultimately influence the macroscopic magnetic properties of the material. This observation not only offers a new perspective for the mechanistic exploration of REFeB magnets, but also suggests that electronegativity could serve as an indicator for optimizing their composition and performance.

3.2.2. Composition optimization

3.2.2.1. Prediction results. Given the uneven distribution of rare earth elements, designing REFeB magnets that incorporate high-abundance elements while maintaining high magnetic properties is essential. La and Ce, among the most abundant rare earth elements in the Earth's crust with concentrations of 63 ppm and 31 ppm respectively [36], offer a more economical alternative to PrNd elements. We utilized the established machine learning models in Section 3.2 together with verification experiments to investigate the correlation between rare-earth content (PrNd, La, Ce) and the magnetic performance of the representative composition $((Pr,Nd)_xLa_yCe_{1-x-y})_{12}Fe_{82}B_6$. Our objective was to identify compositions with high proportions of high-abundance rare earth elements while maintaining optimal magnetic performance, targeting an efficient balance between performance and cost. Using a step size of 2.5 % for x and y, and setting upper and lower limits at 0 % and 100 % respectively, we created a virtual compositional space comprising 825 data points, which represent the ratios of PrNd, La, and Ce elements in the rare earth composition of (PrNd, La, Ce)-Fe-B magnets. To focus on the effect of substituting high-abundance rare earth elements, the concentrations of other elements remain constant at their respective modal values, which corresponds to the virtual compound ((Pr, Nd)$_x$La$_y$Ce$_{1-x-y}$)$_{12}$Fe$_{82}$B$_6$.

Fig. 7 illustrates the distinct correlations between the magnetic performance of (PrNd$_x$La$_y$Ce$_{1-x-y}$)$_{12}$Fe$_{82}$B$_6$ and its rare-earth element content. It is evident that different magnetic properties exhibit distinct behaviors. For coercivity, since the significantly lower intrinsic magnetic properties of the $La_2Fe_{14}B$ and $Ce_2Fe_{14}B$ compared to $Pr_2Fe_{14}B$ and $Nd_2Fe_{14}B$ [37], the intrinsic coercivity of the magnet decreases noticeably as the proportion of La and Ce increases. The contour distribution in the figure indicates that the predominant factor influencing the variation in coercivity is the proportion of PrNd elements among the rare earth elements (Fig. 7a), a higher proportion of PrNd is associated with higher coercivity values, as indicated by the red-colored region. When the proportion of PrNd exceeds 75 %, the predicted coercivity remains above 650 kA/m. Meanwhile, both La and Ce exhibit detrimental effects on coercivity, increased substitution of either element leads to a general decline in coercivity. The remanence map shows significantly larger red-color regions (Fig.7b), primarily due to the effects of La. While an increase in Ce also causes a gentle decrease in remanence, La's impact is even less severe. This difference stems from the higher saturation magnetization of $La_2Fe_{14}B$ compared to $Ce_2Fe_{14}B$, making the substitution of PrNd with La more effective for remanence than using Ce. Our ensemble model accurately captures these nuances, resulting in different predictions for the substitution effects of La and Ce. Previous studies have revealed that synergistic interactions between La and Ce in REFeB magnets can facilitate the transition of Ce to magnetic valence state and restrict the formation of detrimental phases like $CeFe_2$, thereby promoting enhanced remanence [38–40]. The predicted results from our model identified this effect, showing higher values of remanence when La replaces Ce (Fig. 7b). Meanwhile, the relatively high remanence values in the high La substitution areas may also be due to this effect. However, from an industrial application standpoint, magnets must exhibit optimal overall magnetic performance, encompassing high levels of coercivity, remanence, and maximum energy product concurrently. Analysis of the predicted results of maximum energy product reveals that for (PrNd$_x$La$_y$Ce$_{1-x-y}$)$_{12}$Fe$_{82}$B$_6$ magnets, the region with a value higher than 100 kJ/m^3, falls within approximately 25 % to 40 % La, <20 % Ce, and PrNd ranging from 55 % to 75 % (Fig. 7c), which is comparable to the areas with very small La and Ce content. Moreover, within this special compositional window (Region B in Fig. 8a), the magnet demonstrates maximum energy product values exceeding 103 kJ/m^3 while maintaining substantial levels of coercivity (exceeding 469 kA/m) and remanence (exceeding 0.870 T), providing an optimal composition area for high LaCe substituted magnets with good overall magnetic performance. Generally, an optimal *(BH)*$_{\max}$ with high value needs both coercivity and remanence simultaneously have sufficient high values. However, the behaviors of coercivity and remanence usually are competitive in high-abundancy rare earth substituted REFeB magnet, leading to a serious challenge in optimizing their magnetic performance. This predicted optimal composition area indicates that the opposing behaviors of coercivity and remanence under certain conditions can also result in an optimized region with a balanced magnetic performance for LaCe substituted magnets.

To verify the unique nature of this newly-discovered compositional

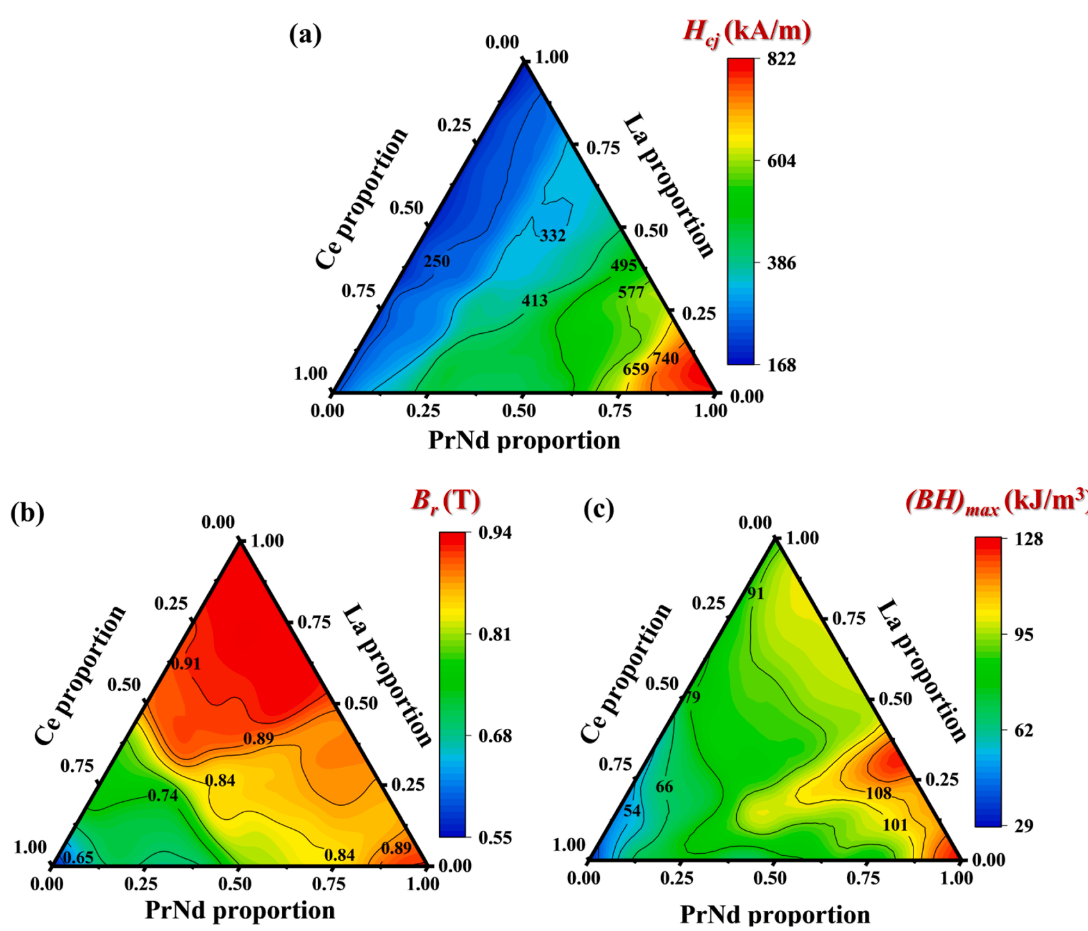

Fig. 7. Ternary contour plots of (a) H_{cj} (b)B_r (c) *(BH)*$_{\max}$ for (PrNd$_x$La$_y$Ce$_{1-x-y}$)$_{12}$Fe$_{82}$B$_6$ magnets.

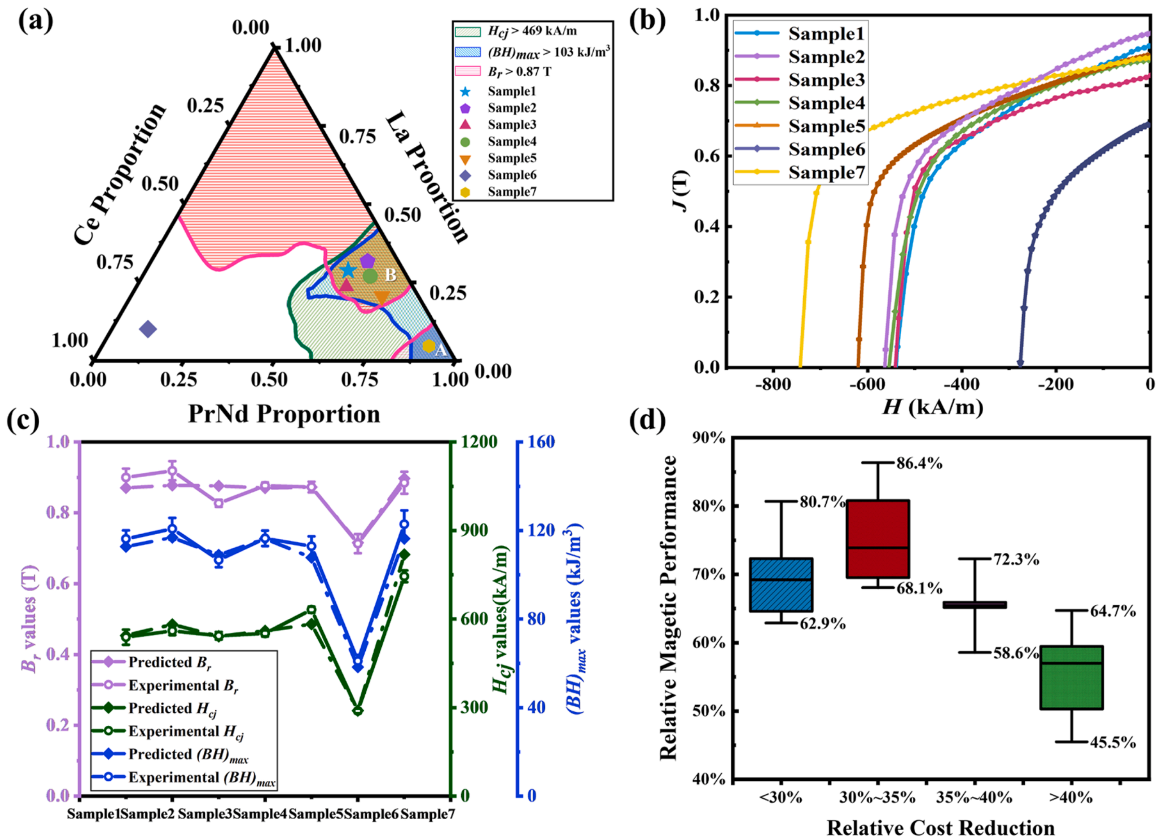

Fig. 8. (a)The high magnetic properties region for $((Pr,Nd)_xLa_yCe_{1-x-y})_{12}Fe_{82}B_6$. (b) Demagnetization curves of selected samples used for verification experiments (c) Comparison of predicted and experimental values for the verification experiments, the mean values of these measurements were taken as the final results for verification experiments, the error bars are calculated from the standard deviation of the magnetic properties of five different samples of the same composition (d) Box plot of relative cost reduction and relative magnetic performance, the upper and lower boundaries of the box represent the interquartile range, the line inside the box represents the median, and the whiskers extending from the box represent the minimum and maximum values.

area, we further calculated the electronegativity parameters for Region B (Supplementary Information, Table S4). The result showed that the electronegativity parameters in Region B fall within the optimal ranges associated with a high $(BH)_{max}$ (EN_{Wsum} ranges from 1.75 to 1.79, EN_{Wdif} from 1.4 to 1.6, EN_{WSvar} between 0.04 and 0.06, and EN_{WDvar} from 0.06 to 0.14), well consistent with the patterns observed in Fig. 6. This result confirms that Region B presents promising magnetic characteristics, warranting further exploration.

3.2.2.2. Experimental verification. To further validate the accuracy of our model predictions, especially for Region B (Fig. 8a), verification experiments were conducted. Seven compositions were selected for verifying, with a focus on five compositions located within Region B in Fig. 8a (sample1 to 5) and two compositions (sample6 and sample7) dispersed outside (Fig. 8a). The experimental measurements show that all seven samples achieve prediction accuracies of over 90 %, as presented in Fig. 8b and c and Table 2. Here, the prediction accuracy is defined as $1 - |M_{exp} - M_{pred}|/M_{exp}$, where M_{exp} represents the experimental value of the samples' magnetic properties, and M_{pred} represents the predicted value. Additional characterization measurement results (XRD patterns and Hysteresis loops) for the validation samples are provided in the supplementary materials.

To account for potential errors introduced during experimental measurements, we assessed the magnetic properties of five independent samples for each composition under identical conditions. The verification results show that the prediction models achieved an accuracy exceeding 90 % for B_r, H_{cj}, and $(BH)_{max}$ across seven randomly selected compositions, demonstrating the model's high reliability in predicting magnetic properties. Notably, for samples within Region B (Sample 1–Sample 5), the model demonstrated even higher predictive accuracy,

Table 2
Verifying experiment results for $((Pr,Nd)_xLa_yCe_{1-x-y})_{12}Fe_{82}B_6$.

	Sample1	Sample2	Sample3	Sample4	Sample5	Sample6	Sample7
Composition	$x = 0.575$, $y = 0.275$	$x = 0.6$, $y = 0.3$	$x = 0.575$, $y = 0.225$	$x = 0.625$, $y = 0.275$	$x = 0.7$, $y = 0.2$	$x = 0.1$, $y = 0.1$	$x = 0.9$, $y = 0.05$
Predicted B_r (T)	0.871	0.878	0.877	0.870	0.873	0.716	0.897
Experimental B_r (T)	0.900±0.025	0.919±0.027	0.827±0.010	0.877±0.009	0.873±0.015	0.713±0.027	0.885±0.031
B_r accuracy	97 %	96 %	94 %	99 %	100 %	99 %	99 %
Predicted H_{cj} (kA/m)	544	582	542	560	583	290	819
Experimental H_{cj} (kA/m)	539±25.5	560±14.3	544±12.7	551±10.3	632±10.3	289±7.96	745±19.9
H_{cj} accuracy	99 %	96 %	99 %	98 %	92 %	99 %	90 %
Predicted $(BH)_{max}$ (kJ/m^3)	113	117	109	116	108	58.3	116
Experimental $(BH)_{max}$ (kJ/m^3)	116±3.82	121±4.93	107±3.26	115±3.50	113±4.46	61.1 ± 2.79	123±6.29
$(BH)_{max}$ accuracy	97 %	97 %	98 %	99 %	96 %	95 %	94 %

exceeding 92 %. Furthermore, the magnetic property predictions for the majority of the samples reached accuracies above 95 %. The predictions for the magnetic energy product exhibited the highest accuracy, while the predictive accuracy for coercivity was slightly lower, though still exceeding 90 %, which validates the accuracy and robustness of our machine learning models.

3.2.2.3. Cost-performance analysis. Verification experiments confirm the reliability of our machine learning models' predictions, particularly highlighting the favorable overall magnetic performance of Region B (Fig. 8a). The results indicate that Region B, characterized by relatively high proportions of La and Ce, holds the potential for industrial valuable and cost-effective magnets. Given these promising findings, we conducted a further cost-effectiveness analysis for this specific region.

To comprehensively analyze the relationship between the overall magnetic performance and material cost of magnets and identify compositions with optimal cost-effectiveness, we used the product of three magnetic properties ($H_{cj} \times B_r \times (BH)_{max}$) to evaluate the overall magnetic performance of magnets. This evaluation provides a more intuitive representation of the variations in the three magnetic properties across different compositions and has also been employed in previous studies [41]. The cost of the magnets was calculated based on the market prices of La at 3426 USD/ton, Ce at 3701 USD/ton, and PrNd at 96,860 USD/ton [42] with the costs of Fe and B being negligible. As a benchmark for comparison, we selected the magnetic performance and cost of $(Pr,Nd)_{12}Fe_{82}B_6$ (without La or Ce substitution).To further validate the reliability of the cost-effectiveness analysis, we further validated the benchmark composition through verifying experiment. The accuracy of the model-predicted magnetic properties compared to the experimental results remains at 90 % for the benchmark composition (Supplementary Material, Table S7, Fig. S6). Based on the obtained results shown in Fig. 7, we computed the relative magnetic performance (based on our predictive results) and relative cost of magnets in Region B, benchmarked against $(Pr,Nd)_{12}Fe_{82}B_6$. The results were statistically analyzed and visualized in Fig. 8d In Region B, the high proportion of abundant rare earth elements La and Ce leads to a significant reduction in the material costs of the magnets, achieving a relative cost reduction of approximately 30–45 %. However, this reduction in cost is accompanied by a decrease in overall magnetic performance. When the relative cost reduction exceeds 35 %, the overall magnetic performance falls below 80 %. But within the range of a 35 % cost reduction, there are some compositions that maintain good overall magnetic performance. Specifically, for the cost reduction below 30 %, the highest relative magnetic performance achieved is 80.7 % of the benchmark magnet. This indicates promising directions for cost-effective compositions. The most notable finding is that a magnet with the composition $(Pr,Nd)_{8.1}La_{3.6}Ce_{0.3}Fe_{82}B_6$, predicted by our machine learning models, exhibits the highest overall magnetic performance, reaching 86.4 % of the benchmark with H_{cj} = 660 kA/m, B_r = 0.880 T, and $(BH)_{max}$ = 128 kJ/m^3, while also achieving a 31.3 % reduction in cost.

Further search of cost-effective compositions targeting ones retaining >80 % of overall magnetic performance yielded three other compositions based on our predictive results: $(Pr,Nd)_{8.1}La_{3.9}Fe_{82}B_6$, $(Pr,Nd)_{8.4}La_{3.6}Fe_{82}B_6$ and $(Pr,Nd)_{8.1}La_{3.3}Ce_{0.6}Fe_{82}B_6$. Compared to the composition without La and Ce substitution, their predicted magnetic performances were retained at 80.8 % (H_{cj} = 614 kA/m, B_r = 0.885 T, $(BH)_{max}$ = 128 kJ/m^3), 80.7 % (H_{cj} = 633 kA/m, B_r = 0.878 T, $(BH)_{max}$ = 125 kJ/m^3), and 81.7 % (H_{cj} = 638 kA/m, B_r = 0.875 T, $(BH)_{max}$ = 126 kJ/m^3), respectively, while reducing the cost by 31.4 %, 28.9 % and 31.3 %, respectively. These compositions exhibit a commendable balance of cost-efficiency and magnetic performance, achieving a substantial substitution of abundant rare earth elements while retaining favorable values of coercivity, remanence, and maximum energy product, which is of significance for the balanced utilization of rare earth elements and the practical application of REFeB magnets. Moreover, these results highlight the efficacy of our machine learning approach in developing cost-effective REFeB permanent magnets and demonstrate its potential to advance material discovery and optimization.

4. Conclusion

In this study, machine learning techniques were employed to optimize the composition design of melt-spun high-abundance REFeB (RE = PrNd, La, Ce) permanent magnets, comprehensively encompassing three magnetic properties of H_{cj}, B_r and $(BH)_{max}$. Sixteen mainstream regression models were screened and then optimized using three heuristic optimization algorithms (GA, PSO, DE). To enhance the models' generalization ability, the ensemble strategy was further introduced, attaining correlation coefficients (R^2) of 0.927 for H_{cj}, 0.932 for B_r, and 0.907 for $(BH)_{max}$.

Using the established ensemble models, we predicted the magnetic performance of REFeB permanent magnets, focusing on the impact of elemental electronegativity and chemical composition. Distinct correlations between electronegativity parameters and magnetic performance were identified, indicating that the statistic electronegativity might be a good indicator for the magnetic performance of REFeB materials. Furthermore, the impact of rare earth element content on the magnetic performance of $((Pr,Nd)_xLa_yCe_{1-x-y})_{12}Fe_{82}B_6$ was investigated based on the ensemble models, with a specific focus on substituting high-abundance rare earth elements La and Ce for PrNd. We discovered a special composition region with optimal overall magnetic performance, with La and Ce ratios reaching up to 40 % and 20 %, respectively. Verification experiments showed that our models' predictions achieved an accuracy rate of over 90 %, validating the excellent overall magnetic performance of this region. A cost-effectiveness analysis was then conducted for this newly-discovered region, and compositions with high cost-effectiveness were identified. Among them, $(Pr,Nd)_{8.1}La_{3.6}Ce_{0.3}Fe_{82}B_6$ achieves a 31.3 % cost reduction while retaining 86.4 % of the overall magnetic performance compared to the corresponding composition without La/Ce substitution. Three other compositions in this region were also identified, achieving approximately 30 % cost reduction while maintaining over 80 % of the magnetic performance: $(Pr,Nd)_{8.1}La_{3.9}Fe_{82}B_6$, $(Pr,Nd)_{8.4}La_{3.6}Fe_{82}B_6$ and $(Pr,Nd)_{8.1}La_{3.3}Ce_{0.6}Fe_{82}B_6$. These findings not only are conducive to the optimization of REFeB magnet compositions, but also demonstrate the enormous potential of machine learning approach in the design and development of high-performance and cost-effective REFeB permanent magnets, which holds significant practical significance. The presented ensemble machine learning method offers a swift and cost-effective approach for optimizing high-abundant REFeB permanent magnets.

CRediT authorship contribution statement

Zheng Wang: Writing – original draft, Methodology, Investigation, Data curation. **Shiyi Zhang:** Validation, Investigation. **Jing Wang:** Writing – review & editing, Supervision, Funding acquisition, Conceptualization. **Ming Zhang:** Investigation. **Yunzhong Chen:** Resources. **Baohe Li:** Validation. **Tongyun Zhao:** Resources. **Minggang Zhu:** Writing – review & editing, Supervision. **Fengxia Hu:** Writing – review & editing, Resources, Funding acquisition. **Baogen Shen:** Supervision, Resources, Funding acquisition. **Wei Li:** Writing – review & editing, Supervision.

Declaration of competing interest

The authors declare that they have no known competing financial interests or personal relationships that could have appeared to influence the work reported in this paper.

Acknowledgements

This work was supported by the National Key Research and Development Program of China (grant nos. 2022YFB3505201, 2023YFA1406003), the High-quality Development Special Funds Program Ministry of Industry and Information Technology (Grant No. TC220H06G), the National Natural Sciences Foundation of China (grant nos. 52088101, 92263202, U23A20550, 22361132534), and the Strategic Priority Research Program (B) of the Chinese Academy of Sciences (XDB33030200).

Supplementary materials

Supplementary material associated with this article can be found, in the online version, at doi:10.1016/j.actamat.2025.121031.

References

[1] M. Sagawa, S. Fujimura, N. Togawa, H. Yamamoto, Y. Matsuura, New material for permanent magnets on a base of Nd and Fe, J. Appl. Phys. 55 (6) (1984) 2083–2087.
[2] J. Coey, Perspective and prospects for rare earth permanent magnets, Engineering 6 (2) (2020) 119–131.
[3] O. Gutfleisch, M.A. Willard, E. Brück, C.H. Chen, S. Sankar, J.P. Liu, Magnetic materials and devices for the 21st century: stronger, lighter, and more energy efficient, Adv. Mater. 23 (7) (2011) 821–842.
[4] H. Sepehri-Amin, Y. Une, T. Ohkubo, K. Hono, M. Sagawa, Microstructure of fine-grained Nd–Fe–B sintered magnets with high coercivity, Scr. Mater. 65 (5) (2011) 396–399.
[5] M. Soderžnik, M. Korent, K. Žagar Soderžnik, M. Katter, K. Üstüner, S. Kobe, High-coercivity Nd-Fe-B magnets obtained with the electrophoretic deposition of submicron TbF3 followed by the grain-boundary diffusion process, Acta Mater. 115 (2016) 278–284.
[6] F. Zhai, A. Sun, D. Yuan, J. Wang, S. Wu, A.A. Volinsky, Z. Wang, Epoxy resin effect on anisotropic Nd–Fe–B rubber-bonded magnets performance, J. Alloy. Compd. 509 (3) (2011) 687–690.
[7] J. Fidler, T. Schrefl, Overview of Nd–Fe–B magnets and coercivity (invited), J. Appl. Phys. 79 (8) (1996) 5029–5034.
[8] X. Fan, S. Guo, K. Chen, R. Chen, D. Lee, C. You, A. Yan, Tuning Ce distribution for high performanced Nd-Ce-Fe-B sintered magnets, J. Magn. Magn. Mater. 419 (2016) 394–399.
[9] C.D. Fuerst, T.W. Capehart, F.E. Pinkerton, J.F. Herbst, Preparation and characterization of La2-Xcexfe14b compounds, J. Magn. Magn. Mater. 139 (3) (1995) 359–363.
[10] A.K. Pathak, M. Khan, K.A. Gschneidner, R.W. McCallum, L. Zhou, K. Sun, K. W. Dennis, C. Zhou, F.E. Pinkerton, M.J. Kramer, V.K. Pecharsky, Cerium: an unlikely replacement of dysprosium in high performance Nd–Fe–B permanent magnets, Adv. Mater. 27 (16) (2015) 2663–2667.
[11] I. Poenaru, A. Lixandru, K. Güth, A. Malfliet, S. Yoon, I. Škulj, O. Gutfleisch, HDDR treatment of Ce-substituted Nd2Fe14B-based permanent magnet alloys - phase structure evolution, intergranular processes and magnetic property development, J. Alloy. Compd. 814 (2020).
[12] D. Dai, Q. Liu, R. Hu, X. Wei, G. Ding, B. Xu, T. Xu, J. Zhang, Y. Xu, H. Zhang, Method construction of structure-property relationships from data by machine learning assisted mining for materials design applications, Mater. Des. 196 (2020).
[13] K. Hamidieh, A data-driven statistical model for predicting the critical temperature of a superconductor, Comput. Mater. Sci. 154 (2018) 346–354.
[14] T. Konno, H. Kurokawa, F. Nabeshima, Y. Sakishita, R. Ogawa, I. Hosako, A. Maeda, Deep learning model for finding new superconductors, Phys. Rev. B 103 (1) (2021).
[15] B. Meredig, E. Antono, C. Church, M. Hutchinson, J. Ling, S. Paradiso, B. Blaiszik, I. Foster, B. Gibbons, J. Hattrick-Simpers, A. Mehta, L. Ward, Can machine learning identify the next high-temperature superconductor? Examining extrapolation performance for materials discovery, Molecul. Syst. Des. Eng. 3 (5) (2018) 819–825.
[16] V. Stanev, C. Oses, A.G. Kusne, E. Rodriguez, J. Paglione, S. Curtarolo, I. Takeuchi, Machine learning modeling of superconducting critical temperature, Npj Comput. Mater. 4 (2018).
[17] Y.-J. Chang, C.-Y. Jui, W.-J. Lee, A.-C. Yeh, Prediction of the composition and hardness of high-entropy alloys by machine learning, Jom 71 (10) (2019) 3433–3442.
[18] Y. Li, W. Guo, Machine-learning model for predicting phase formations of high-entropy alloys, Phys. Rev. Mater. 3 (9) (2019).
[19] Z. Rao, P.-Y. Tung, R. Xie, Y. Wei, H. Zhang, A. Ferrari, T.P.C. Klaver, F. Koermann, P.T. Sukumar, A.K. da Silva, Y. Chen, Z. Li, D. Ponge, J. Neugebauer, O. Gutfleisch, S. Bauer, D. Raabe, Machine learning-enabled high-entropy alloy discovery, Science 378 (6615) (2022) 78–84.
[20] C. Wen, Y. Zhang, C. Wang, D. Xue, Y. Bai, S. Antonov, L. Dai, T. Lookman, Y. Su, Machine learning assisted design of high entropy alloys with desired property, Acta Mater. 170 (2019) 109–117.
[21] Q. Wu, Z. Wang, X. Hu, T. Zheng, Z. Yang, F. He, J. Li, J. Wang, Uncovering the eutectics design by machine learning in the Al-Co-Cr-Fe-Ni high entropy system, Acta Mater. 182 (2020) 278–286.
[22] J. Yang, F. Shi, C. Zhou, S. Zhang, Q. Sui, L. Chen, Machine learning and theoretical prediction of highly spin-polarized Cr2COx MXene with enhanced curie temperature, Adv. Funct. Mater. 34 (52) (2024) 2411170.
[23] S. Lu, Q. Zhou, Y. Guo, Y. Zhang, Y. Wu, J. Wang, Coupling a crystal graph multilayer descriptor to active learning for rapid discovery of 2D ferromagnetic semiconductors/half-metals/metals, Adv. Mater. 32 (29) (2020) 2002658.
[24] Y. Wang, Y. Tian, T. Kirk, O. Laris, J. R. Noebe Jr, V. Keylin, R. Arroyave, Accelerated design of Fe-based soft magnetic materials using machine learning and stochastic optimization, Acta Mater. 194 (2020) 144–155.
[25] W. Guo, Y. Wu, L. Shi, J. Jia, R. Wang, H. Bu, Z. Zhu, Y. Shao, K. Yao, Integrating ultra-high saturation magnetization intensity and extreme-low coercivity in FeCoBSiCu alloy assisted by machine learning, Acta Mater. 285 (2025) 120643.
[26] G. Xu, Cheng F, H. Lu, C. Hou, X.-Y. Song, Predicting the Curie temperature of Sm-Co-based alloys via data-driven strategy, Acta Mater. 274 (2024) 120026.
[27] A.K. Choudhary, T. Grubesa, A. Jansche, T. Bernthaler, D. Goll, G. Schneider, Deep learning and correlative microscopy for quantification of grain orientation in sintered FeNdB-type permanent magnets by domain pattern analysis, Acta Mater. 264 (2024) 119563.
[28] J. Jiang, H. Du, W. Zhang, Electronegativity, atomic pseudoradii and rare earth permanent magnet materials, J. Chin. Rare Earth Soc. 21 (3) (2003) 287–290.
[29] H.A. Eiselt, C.L. Sandblom, Heuristic algorithms, in: H.A. Eiselt, C.L. Sandblom (Eds.), Integer Programming and Network Models, Springer, Berlin Heidelberg, Berlin, Heidelberg, 2000, pp. 229–258.
[30] S. Katoch, S.S. Chauhan, V. Kumar, A review on genetic algorithm: past, present, and future, Multimed. Tool. Appl. 80 (5) (2021) 8091–8126.
[31] M.F. Ahmad, N.A.M. Isa, W.H. Lim, K.M. Ang, Differential evolution: a recent review based on state-of-the-art works, Alex. Eng. J. 61 (5) (2022) 3831–3872.
[32] A.G. Gad, Particle swarm optimization algorithm and its applications: a systematic review, Arch. Comput. Method. Eng. 29 (5) (2022) 2531–2561.
[33] I.D. Mienye, Y. Sun, A survey of ensemble learning: concepts, algorithms, applications, and prospects, IEEE Access 10 (2022) 99129–99149.
[34] F. Pedregosa, G. Varoquaux, A. Gramfort, V. Michel, B. Thirion, O. Grisel, M. Blondel, P. Prettenhofer, R. Weiss, V. Dubourg, J. Vanderplas, A. Passos, D. Cournapeau, M. Brucher, M. Perrot, E. Duchesnay, Scikit-learn: machine learning in Python, J. Mach. Learn. Res. 12 (2011) 2825–2830.
[35] J. Blank, K. Deb, Pymoo: multi-objective optimization in Python, IEEE Access 8 (2020) 89497–89509.
[36] B. Zhou, Z. Li, C. Chen, Global potential of rare earth resources and rare earth demand from clean technologies, Minerals 7 (11) (2017) 203.
[37] J.F. Herbst, R2FE14B Materials - intrinsic-properties and technological aspects, Rev. Mod. Phys. 63 (4) (1991) 819–898.
[38] G. Delette, Nd2Fe14B permanent magnets substituted with non-critical light rare earth elements (Ce, La): a review, J. Magn. Magn. Mater. 577 (2023) 16.
[39] Z. Li, M. Yue, X.B. Liu, H.G. Zhang, W.Q. Liu, Y.Q. Li, Z.P. Zhang, Tuning the structure and intrinsic magnetic properties of $Ce_2Fe_{14}B$ alloys by elimination of $CeFe_2$ with La substitution, J. Magn. Magn. Mater. 505 (2020) 7.
[40] J.Y. Jin, Y.J. Zhang, G.H. Bai, Z.Y. Qian, C. Wu, T.Y. Ma, B.G. Shen, M. Yan, Manipulating Ce valence in $RE_2Fe_{14}B$ tetragonal compounds by La-Ce Co-doping: resultant crystallographic and magnetic anomaly, Sci. Rep. 6 (2016) 9.
[41] J. Chen, J. Liu, M. Zhang, Z. Dong, Z. Peng, X. Ji, M. Liu, L. Zhang, A. Zhang, H. Zhu, Accelerated discovery of cost-effective Nd–Fe–B magnets through adaptive learning, J. Mater. Chem. A 11 (16) (2023) 8988–9001.
[42] There are fluctuations in rare earth prices, so we chose the April 2023 prices as a median for our calculations, the price data was from RARE EARTH INFORMATION 04(2024) and converted to the US dollar before the calculation.